25th ABCM International Congress of Mechanical Engineering
October 20-25, 2019, Uberlândia, MG, Brazil

COBEM2019-2409
CHARACTERIZATION OF CORROSION WITHIN FRICTION STIR WELD ZONES OF AN API X-70 STEEL

Juliane Ribeiro da Cruz
Mechanical Engineering Department, Aeronautics Institute of Technology (ITA), Praça Marechal Eduardo Gomes, 50, 12228-900, São José dos Campos, Sao Paulo, Brazil
juliane.rcruz@gmail.com

Rodnei Bertazzoli
Faculty of Mechanical Engineering, State University of Campinas, Mendeleyev, 200, 13083-860, Campinas, São Paulo, Brazil
rbertazzoli@fem.unicamp.br

Abstract. *The susceptibility of API-X70 friction stir weld zones to corrosion in Na_2SO_4 acid media is investigated using an electrochemical microcell. Potential galvanic couples between the weld zones and the preferential corrosion sites were identified. The most anodic zone was base metal that, with a banded microstructure of ferritic and perlitic grains, developed a potential difference of up to 45 mV in comparison to the adjacent heat affected zone. Hard zone was the second most anodic region and, with fine bainitic structure, developed a corrosion potential difference of 37 mV toward the adjacent thermomechanical affected zone (TMAZ), the most cathodic zone. The best combination of parameters for corrosion resistance was obtained at microstructures with both acicular ferrite and coarse bainite, as TMAZ and stir zone, that presented high corrosion potentials, polarization resistances and Tafel slopes. Although fine bainitic structure of hard zone developed the smallest corrosion current densities, its lower corrosion potential and higher sensitivity to potential variation (small Tafel slopes) eventually led to pitting corrosion at grain boundaries. Corrosion current density slightly decreased from base metal toward stir zone, while polarization resistance slightly increased. Microstructure refinement and homogenization accounted for this improvement with a more uniform distribution of corrosion products and possible reduction of galvanic corrosion between ferrite and cementite.*

Keywords: *Pipeline steel, Mild steel, capillary-based droplet microcell, weld zones, FSW processing*

1. INTRODUCTION

As a promising solid-state joining process from the decade of 1990, friction stir welding (FSW) quickly gained operational parameters that ensured the quality of welded joints in light metals, mainly aluminum alloys (Mishra and Ma, 2005; Padhy et al., 2018). In the last decade, developments in tool composition and equipment technology have enabled this technique to be applied to high-temperature alloys and steels (Defalco and Steel, 2009). Since then, FSW application for welding of high strength low alloy (HSLA) pipeline API 5L steels, used in the oil and gas industry, has been extensively studied (Padhy et al., 2018; Defalco and Steel, 2009; Santos et al., 2010). Literature reports have been searching for better understanding of FSW processing and bainitic transformation of pipeline steels, to optimize mechanical properties and fracture toughness for large scale structural applications (Santos et al., 2010, Aydin and Nelson, 2013; Sowards et al., 2015; Avila et al., 2016; Pao et al., 2007). However, as pipeline steels can carry or be exposed to environmental corrosive media, there is still a need for a more comprehensive understanding of the friction stir weld performance, especially regarding the electrochemical response of the weld zones, in which metallurgical transformations can multiply active sites and have a detrimental effect on corrosion resistance (Ralston et al., 2010; Jangir et al., 2018).

The weld bead formed by FSW exhibits zones with different microstructures, depending on the thermomechanical cycle imposed along the weld profile. The FSW joint is typically constituted by four zones: (a) base metal (BM), (b) heat affected zone (HAZ), where no plastic deformation takes place, (c) thermo-mechanically affected zone (TMAZ), where material is affected by both heat and plastic deformation, and (d) stir zone (SZ) where a continuous recrystallization takes place during processing. Besides, within the stir zone, microstructure can still change from the advancing to the retreating side of the tool. The advancing side is the side where the velocity vectors of tool rotation and tool travel direction are the same. In the retreating side, however, these vectors are opposite (Mishra et al., 2014). As processed material tends to be left behind as the tool advances, shearing in the advancing side opposes to this flow, while shearing in the retreating side favors this material flow to behind the tool. This way, maximum shearing, strain and peak temperature occur in the advancing side (Mishra et al., 2014). Such behavior results in a sharp microstructure

change between the nugget and TMAZ in the advancing side, while no such clear boundary can be seen in the retreating side (Mishra et al., 2014). The various microstructures within the weld profile of HSLA pipeline steels have been fully reported (Aydin and Nelson, 2013; Sowards et al., 2015; Avila et al., 2016; Pao et al., 2007). Microstructure differences, such as grain size and local phase transformations, can cause the weld zones to react differently under mechanical loading. In fact, microstructure and mechanical properties, such as tensile strength, microhardness, fracture toughness, are highly dependent on the heat input established by the welding parameters, as spindle speed, welding speed and downward force (Aydin and Nelson, 2013; Sowards et al., 2015; Avila et al., 2016; Pao et al., 2007). Such local differences may generate galvanic couples in aqueous oxidizing medium and result in localized corrosion. Besides, in cases when the weld is subjected to mechanical loading or residual stress, stress corrosion cracking may also occur.

Electrochemical characterization of weld zones often requires dispendious sample preparation to section and prepare each individual region for conventional large area characterization. Nevertheless, characterization of short-ranged weld zones, such as thermo-mechanically affect zone, may be even more difficult or impractical. In this case, the working electrode area should be reduced to smaller sizes than the target region to enable space resolution and provide access to local electrochemical information, which demands a micro-cell. Electrochemical micro-cell system was introduced in the 1990s (Böhni et al., 1995; Suter et Böhni, 1997) and has evolved to date through several versions, some of them marketed, as already reviewed (Andreatta and Fedrizzi, 2016). The definition of the working electrode area is a key factor for measurements accuracy. In scanning methods, for instance, the local corrosion current cannot be recorded as there is a contribution of the whole immersed surface. Therefore, the small area technique, in which a glass microcapillary is filled with the electrolyte, is far the most used. In the free drop version, the diameter of the droplet between the capillary and the sample surface defines the area. In the other version, the capillary mouth is coated with silicone that, in contact with the surface of the sample, avoids electrolyte leakage and defines the area.

Jariyaboon and co-authors (Jariyaboon et al., 2006; Jariyaboon et al., 2007; Jariyaboon et al., 2009; Jariyaboon et al., 2010) have reported the effects of FSW on the electrochemical behavior of welding bead zones of aluminum alloys. Except by this series of papers, reports on investigation of corrosion phenomena in FSW weld beads using electrochemical microcells are scarce or even none, especially on FSW of HSLA, API 5L X65 to 80 steels.

In this paper, we investigate the electrochemical response of individual weld zones of an API X-70 friction stir welded pipeline steel in Na_2SO_4 acid media. To perform this task, a novel capillary-based three-electrode microcell was assembled and used. In this microcell, microcapillary consisted in a laser perforated PET (polyethylene terephthalate) mask with micrometric diameters, positioned on the surface of the sample, upon which an electrolyte droplet is deposited. Results from micro and macro scales polarizations are compared. Electrochemical results are discussed and correlated to microstructure and mechanical properties found within the weld zones.

2. MATERIALS AND METHODS

Samples of API-X70 steel with 500 x 95 x 9.5 mm were butt welded on transverse direction by friction stir welding using a PCBN tool (shoulder diameter of 25 mm and pin height of 9.5 mm), 300 rpm, 100 $mm.min^{-1}$ and Z axis force of 33 kN. A weld sample was extracted for microstructure, mechanical and electrochemical characterization. Sample surface was milled for parallelism, causing a thickness reduction from 9.5 to 9.15 mm.

For microstructure characterization, transversal and top surfaces of specimen were grinded from 120 to 1200 mesh, polished with 1 and 0.3 µm alumina and etched with 2% Nital. Microstructure of base metal and weld profile was investigated by optical and scanning electron microscopy (SEM). The nominal chemical composition of API 5L X-70 is presented in Table 1.

Table 1 - Nominal chemical composition of API 5L X-70 steel* (wt%)

C	P	S	Ti	Mn	Fe	Nb	V
0.17	0.02	0.01	0.06	1.75	97.84	0.05	0.1

*http://www.api5lx.com/api5lx-grades/

Vickers microhardness mapping was carried out on top and transversal surfaces of polished weld sample. Indentations were performed under 500g load and every 0.5 mm in both longitudinal and transversal directions.

The electrochemical micro characterization was performed using a potentiostat (Autolab PGSTAT204) and an in-house developed capillary-based microcell. Microcapillary is formed through the hole of a laser drilled adhesive PET (polyethylene terephthalate) mask, positioned on the surface of the working electrode, upon which a droplet of electrolyte is deposited. The electrolyte solution, which consisted in about 30 µL of 0.1 $mol.L^{-1}$ Na_2SO_4 pH 4 solution (adjusted with H_2SO_4 additions), was deaerated by N_2 gas bubbling. Within the electrolyte droplet, micro-sized counter and pseudo-reference electrodes are positioned. Counter electrode (CE) consisted in a platinum wire, with 100 µm of diameter, and the pseudo-reference electrode (RE) consisted in an oxidized tungsten wire, with 125 µm of diameter. A scheme of the microcell is presented in Fig. 1. The tungsten electrode was oxidized in 0.1 $mol.dm^{-3}$ H_2SO_4 solution, from 0.95 to 1.85 volts (vs Ag/AgCl, KCl sat.), for a 100 cycles, following type B procedure, reported by Pasti et al.

(2012). The potential of the anodized tungsten electrode in the Na_2SO_4 electrolyte solution, was -0,124 V versus the Ag/AgCl (KCl sat.) reference electrode. The capillary diameter, determined by the size of mask hole, was of 250 µm (area of 49.0×10^{-5} cm^2). The masks were manufactured by single pulse laser drilling of a typical three-layer PET film, with silicone adhesive on intermediate layer. After removal of top and bottom layers, the mask thickness was of about 0.16 mm. Drilling was performed with a CO_2 Laser with gaussian beam under 100 W power, 180 µm focal diameter and 1 pulse of 1 ms. Five different weld zones were characterized on transversal profile of the weld. Electrochemical characterization was performed in the polished and lightly etched condition, for better contrast among weld zones. In addition, for a more precise positioning of the mask, Vickers indentations were performed within each weld zone, beside which the analysis were performed. Open circuit potential was measured until stabilization (most often achieved after 300 s) for up to 1800 s. This was followed by linear potential scan recorded from -0.6 to -0.3V vs W oxidized electrode (-0.724 to -0.424V vs Ag/AgCl KCl sat. electrode). Potential scan rate was of 1mV/s with acquisition every 0.2mV. At least three replicas were performed for each weld zone. Electrochemical tests were performed inside a Faraday cage in which relative humidity was kept at 75±3%, to minimize electrolyte evaporation.

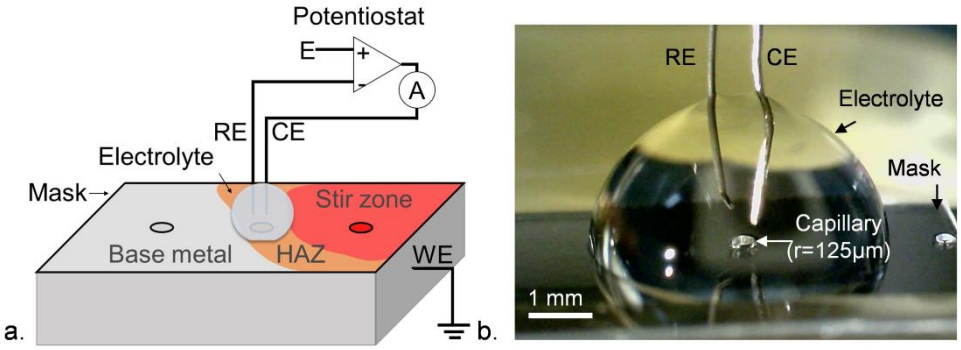

Figure 1. (a) Scheme of the three-electrode capillary-based microcell for electrochemical micro characterization of friction stir weld profile and (b) 30 µL electrolyte drop with reference and counter electrodes.

3. RESULTS AND DISCUSSIONS

3.1 Microstructure of Friction Stir Weld Profile

A macrograph of friction stir weld is shown in Fig. 2. Optical microscopy images of base metal, heat affected zone, thermo-mechanically affected zone and stir zone are presented in Fig. 3. In Fig. 3a, it is possible to see that base metal presented a strongly banded microstructure, composed of ferritic (light) and perlitic (dark grains). Although banding is still present throughout HAZ and TMAZ, Fig. 3b and 3c, diffusion induced by FSW processing attenuated it. In stir zone, banding was eliminated by thermo-mechanical processing. Banding originates at the casting stage of steel manufacture, when carbon and impurities partition to the remaining liquid phase at interdendritic regions and, eventually, line up at the lamination stage. In Fig. 3c, the identification of the thermo-mechanically affected zone is evinced by a shift in banded microstructure direction.

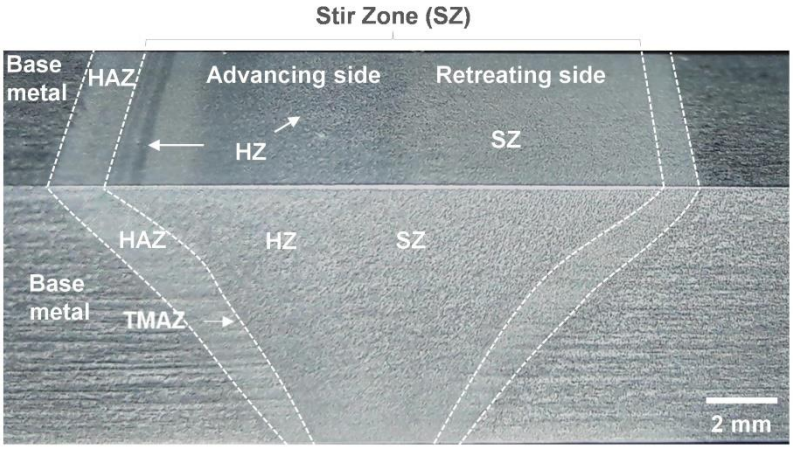

Figure 2. Macrograph of API 5L X-70 friction stir weld showing different weld zones on transversal and top surfaces (HAZ: Heat affected zone, TMAZ: Thermo-mechanically affected zone, HZ: Hard zone and SZ: Stir zone).

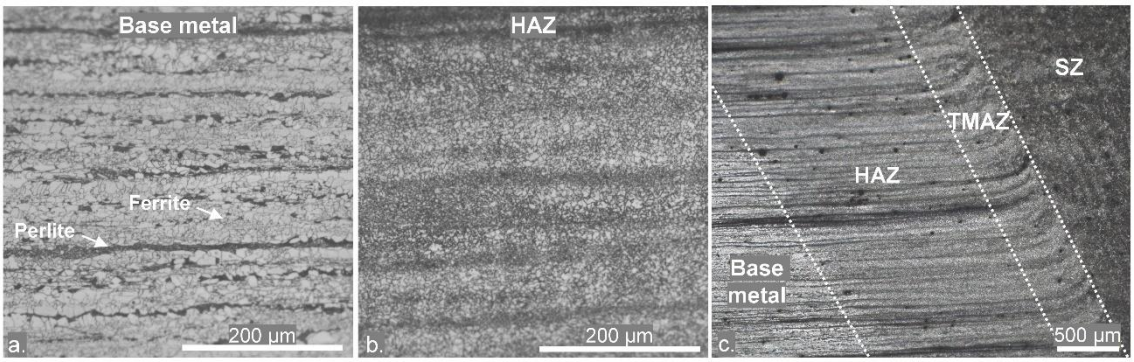

Figure 3. Optical micrographs on cross-section of friction stir weld showing (a) base metal with banded structure, composed of ferritic and perlitic grains, (b) heat affected zone structure with reduced banding due to diffusion and (c) the presence of thermo-mechanically affected zone between HAZ and stir zone

Figure 4 shows the microstructures of different zones on the profile of the friction stir weld (Fig. 2), by scanning electron microscopy. SEM images show that microstructure of base metal is essentially composed of polygonal grains of ferrite and perlite, while, at HAZ, perlite was degenerated by heat-induced diffusion. As diffusion was insufficient to promoted complete homogenization of microstructure, banding remained. At the thermo-mechanically affected zone, recrystallization occurred, and the banded structure of ferrite and perlite turned into a banded structure of acicular ferrite and bainite. In stir zone, microstructure is composed of acicular ferrite and coarse bainite. Microstructure of this zone differs from that of TMAZ in the distribution of bainitic phase. In stir zone, while bainitic phase is evenly distributed among acicular ferrite, in TMAZ, bainitic grains are most likely concentrated along carbon enriched zones of the banded structure. Nevertheless, in the advancing side of stir zone, hard zones with fine bainitic structures were found. This nomenclature agrees with microhardness findings, Fig. 5, in which hard zone exhibited the highest values of microhardness, reaching up to 370 HV. Massive bainite formation on the advancing side is caused by the higher cooling rates achieved in this location because of maximum heat generation due to weld metal shearing with the tool pin and shoulder. The formation of a bainitic hard zone in advancing side of stir zone, agrees with prior reports on mechanical properties of friction stir welds of API X80 steels (Sowards et al., 2015; Avila et al. 2016).

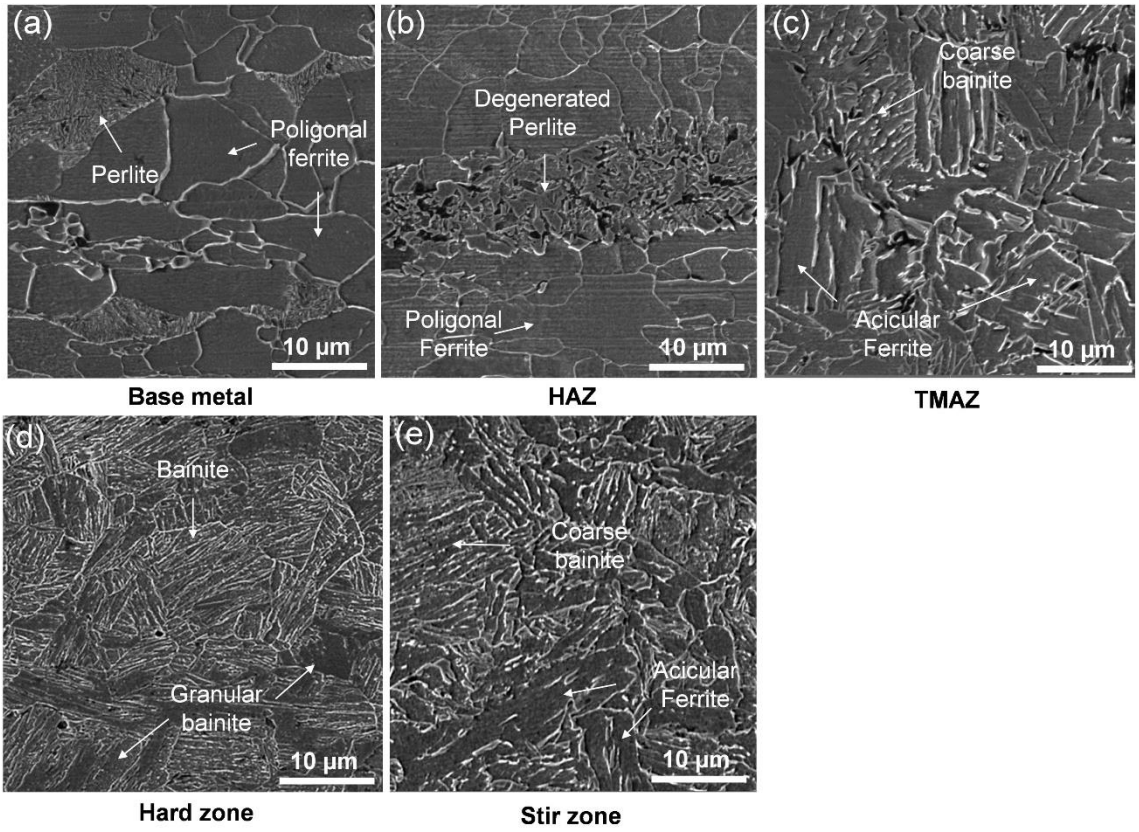

Figure 4. Microstructure of the different weld zones of friction stir weld profile (5kx)

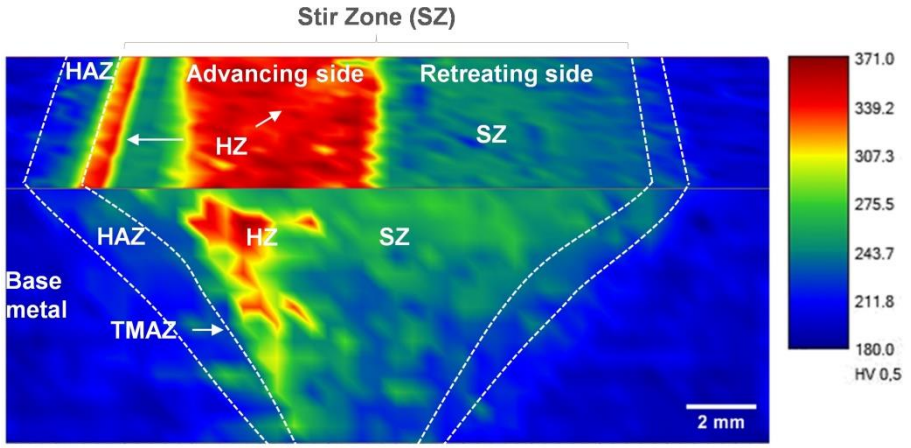

Figure 5. Friction stir weld Vickers microhardness map showing progressive increase in microhardness from base metal (banded microstructure with ferrite and perlite) towards stir zone (coarse bainite and acicular ferrite microstructure). Maximum microhardness is found at hard zone (advancing side of stir zone) due to formation of fine bainitic structure

3.2 Electrochemical Response of Friction Stir Weld Zones

Open circuit potential measurements and polarization curves obtained for the different weld zones are shown in Fig. 6, where the same scales are used for direct comparison. It can be observed that OCP presented fast stabilization and that the shape of polarization curves is similar for all weld zones. In the anodic branch, a Tafel region is observed at low overpotentials. This is followed by two different slope segments at higher overpotentials related to the process of surface pseudo-passivation in sulfate solution. Although soluble, Fe (II) and Fe (III) aquo-complexes must be transported through the diffusion layer at metal/electrolyte interface and, as overpotential increases, iron species formation rate can become greater than mass transfer rate. The difference between the two rates causes the iron species to accumulate on the surface, thus polarizing the corrosion cell and causing the pseudo passivation plateau. Fig. 7 shows the parameters obtained from Tafel analysis for each weld zone. Base metal was the less noble region and presented more negative OCP and E_{corr} than other weld zones, Fig. 7a. Corrosion potential difference between base metal and the adjacent HAZ reached up to about 45mV, where HAZ presented more positive OCP and E_{corr}. This result indicates that, in case of galvanic corrosion, the least damaging condition would be stablished and HAZ would be preserved as base metal corrosion would progress slowly. The second most anodic region is hard zone, with a corrosion potential difference of up to 25mV versus stir zone, and up to 37 mV versus TMAZ, the most cathodic zone. The progressive increase of OCP and E_{corr} toward TMAZ may be related to an increase in cementite surface area due to carbon diffusion and grain refinement, as it was demonstrated that carbon additions shift corrosion potential of steels to more positive values (Ferhat et al., 2014). On the other hand, microstructure refinement is also associated with higher content of lattice defects that, in turn, can account for an increase in steel activity and shift OCP and E_{corr} to more negative values. Results show that optimum condition regarding corrosion potential was achieved at TMAZ and suggest that bainite formation can have a detrimental effect on OCP and E_{corr}, as evinced by HZ and SZ of Fig. 7a, due to a higher surface activity. The higher content of lattice defect in this microstructure is also supported by microhardness measurements that confirm higher hardness and therefore, higher dislocation densities, in this region.

On the other hand, bainitic structure seem to have had a positive effect corrosion current density and polarization resistance. Although corrosion current densities presented the same order of magnitude, a clear tendency in reduction was observed from base metal toward hard zone, where minimum corrosion current density was found, Fig. 7b. Concomitantly, polarization resistance presented a tendency to increase toward stir zone, Fig. 7c. This can be associated with the progressive microstructure refinement and homogenization on weld profile toward stir zone. It has been reported that, when ferrite and perlite are better differentiated (as in banded structure), the galvanic effect between ferrite and cementite is increased (Ochoa et al., 2015) and that a uniform distribution of the phases reduces local anodic/cathodic ratio (Alizadeh and Bordbar, 2013). Besides, a more refined microstructure and a better phase distribution account for the formation of a more compact and uniform passive layer (Alizadeh and Bordbar, 2013; Gollapudi, 2012). This agrees with SEM observations of the corroded microareas that showed better distribution of corrosion products in HA and SZ, than in base metal, HAZ and TMAZ, Fig. 8.

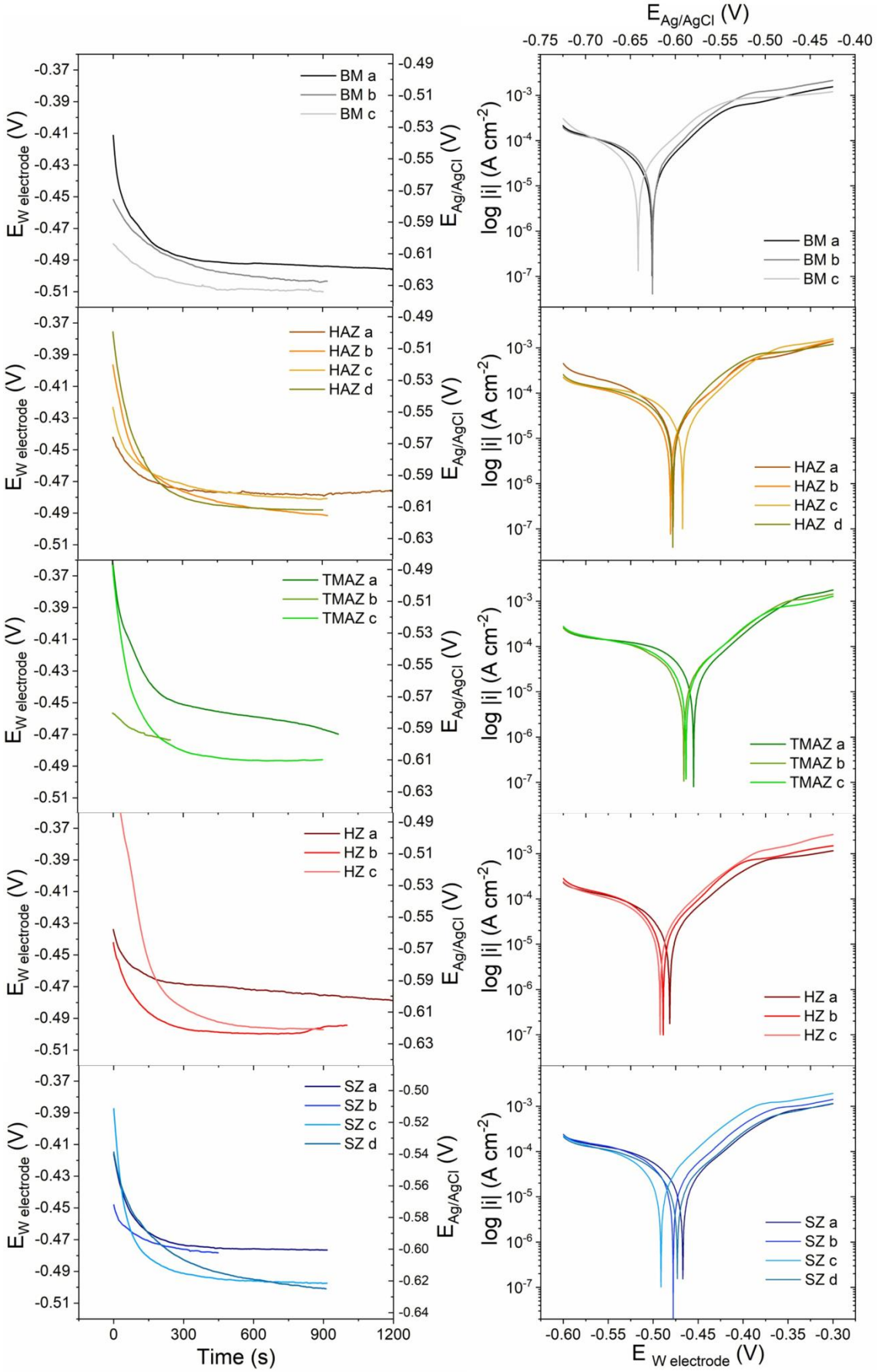

Figure 6. Open circuit potential and polarization curves recorded on micro areas of different weld zones along the friction stir weld profile of API X-70 steel

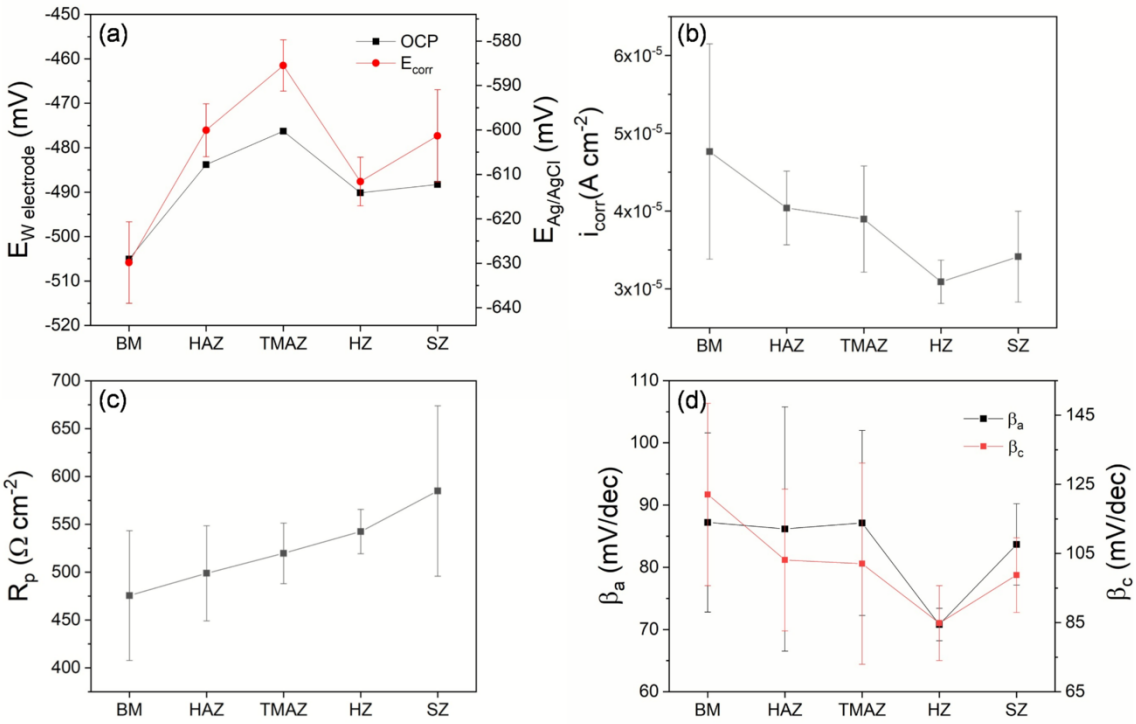

Figure 7. Comparison of Tafel parameters obtained for different weld zones along the friction stir weld profile of API X-70 steel

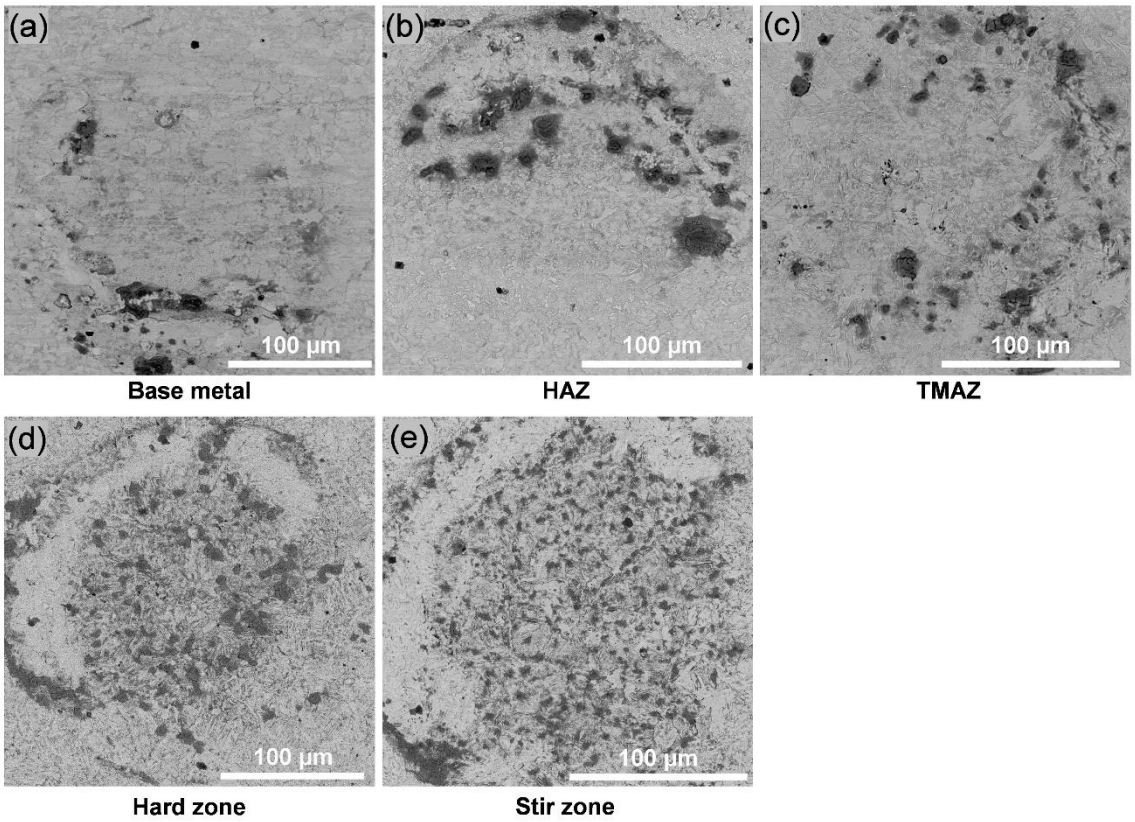

Figure 8. Scanning electron microscopy (back scattered electron) of corrosion product (dark areas) distribution within the weld zones after micro area polarization, showing better distribution of corrosion products in HZ and SZ

Weld zones presented similar anodic and cathodic Tafel slopes, Fig. 7d (βa and βc, respectively), except for hard zone, whose average Tafel slopes were smaller. This shows that current density of hard zone is more sensitive to potential variations. This can result from its higher activity in combination with a progressive increase in galvanic effect, because as the anodic ferritic phase corrodes, the surface area of the cathodic remaining cementite increases (Hao

et al., 2016). This is coherent with microscopy analysis findings, Fig. 9, that show that the grain boundaries of bainitic structure is a susceptible site for pitting corrosion. Fig. 9 shows the morphology of corrosion after simultaneous polarization of the weld zones up to -400mV (vs Ag/AgCl). All weld zones were subjected to general corrosion but, like the grain boundaries of bainitic structure, the perlitic structure (Fig. 9a) and was also more susceptible to pitting corrosion. In perlite, cementite is electrochemically more stable than ferrite and its presence enhances ferrite corrosion by a galvanic effect (Du et al, 2008). Although galvanic corrosion between cementite and ferrite can still be a corrosion trigger within bainite grains, results suggest that solute redistribution and grain refinement by stirring and recrystallization improved corrosion resistance of this region. It is also supported by the fact that pitting was rather found at grain boundaries (most active regions due to dislocation accumulation) than within the bainitic grain itself. Particles detached from FSW tool were found in stir zone (Fig. 10) but did not stood as preferential sites for corrosion.

Interestingly, it can be said that, in general, stir zone presented an intermediate behavior between TMAZ (composed of acicular ferrite with banded bainite) and hard zone (fine bainite), Fig. 7. This is coherent with microstructure found in stir zone, that is composed of both bainite and acicular ferrite.

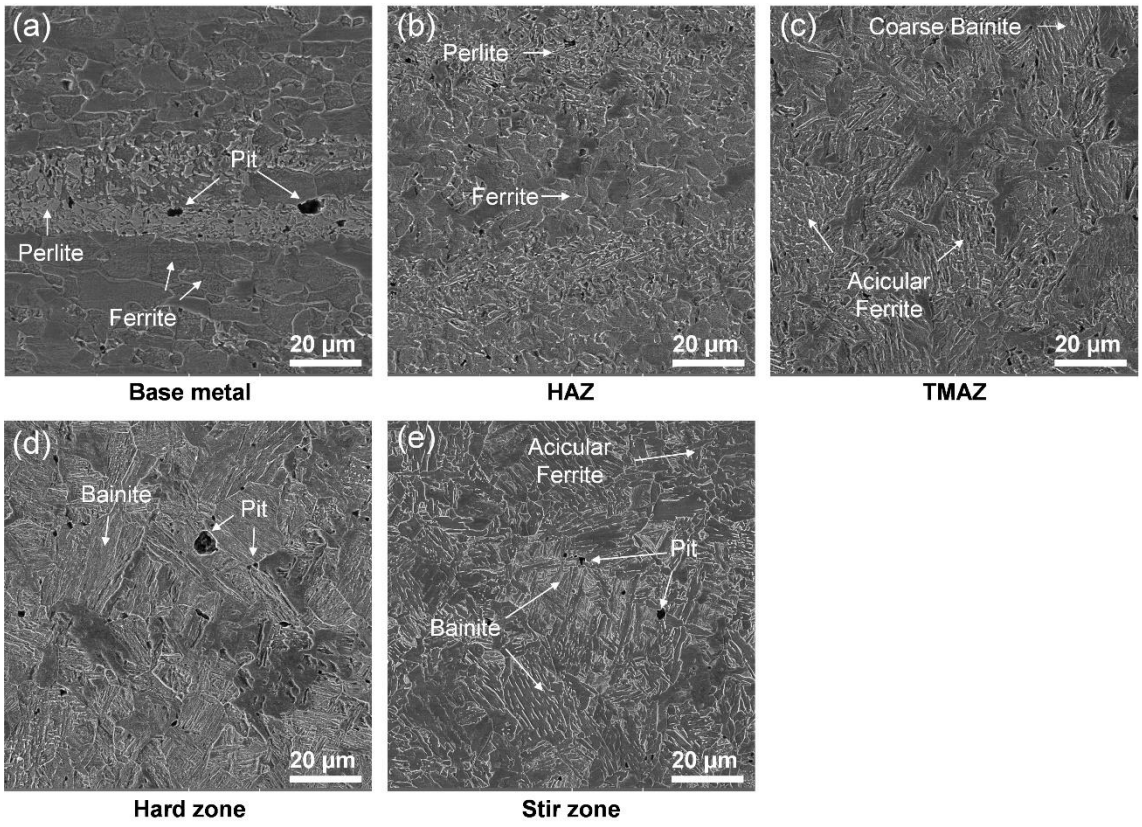

Figure 9. Morphology of corrosion after simultaneous polarization up to -400mV showing general corrosion of weld zones, and pitting corrosion (a) within perlitic structure and (d and e) at bainitic grain boundaries

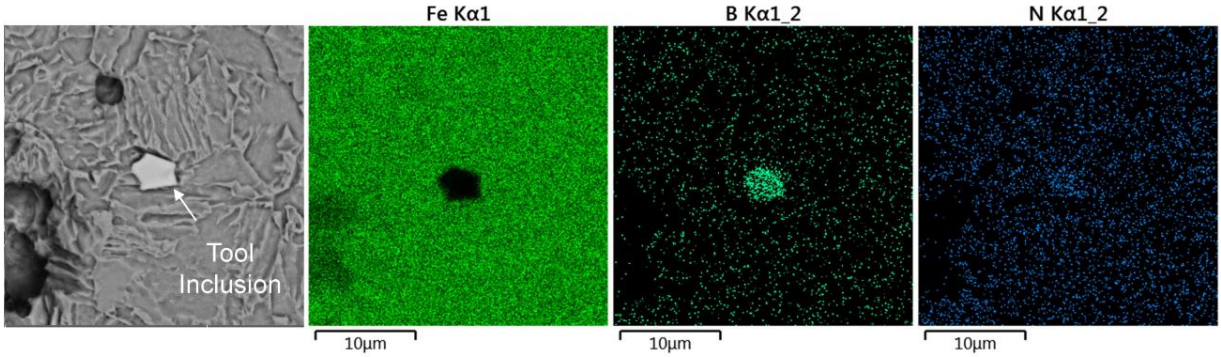

Figure 10. Backscattered electron image of polycrystalline boron-nitride (PCBN) tool inclusion in stir zone. No preferential corrosion occurred around these inclusions

4. CONCLUSIONS

A novel set up of a microcapillary electrochemical droplet cell is presented and used to characterize the susceptibility of API-X70 friction stir weld zones to corrosion in Na_2SO_4 acid media. Potential galvanic couples between the weld zones, that can possibly trigger the corrosive process, and the preferential corrosion sites are identified.

Five different zone developed on weld profile: (1) Base metal, with banded microstructure of polygonal ferritic and perlitic grains, (2) HAZ, with banded structure of polygonal ferrite and degenerated perlite, (3) recrystallized TMAZ, with banded structure of acicular ferrite and bainite, (4) hard zone (on the advancing side of stir zone), with fine bainitic structure, and (5) stir zone, with acicular ferrite and coarse bainite.

Base metal presented the most anodic behavior in comparison to other weld zones. Corrosion potential difference with the adjacent heat affected zone, reached up to 45 mV. In case of galvanic corrosion, this could be considered the least damaging conditions, as HAZ would be preserved in detriment of base metal slow corrosion. The second most anodic zone is hard zone. Corrosion potential difference with adjacent TMAZ and SZ reached up to 37 and 25mV, respectively.

Although base metal and hard zone developed general corrosion, the perlitic structure and bainitic grain boundaries were the most susceptible sites for pitting corrosion. While corrosion current density tended to decrease from base metal toward stir zone, polarization resistance tended to increase. Microstructure refinement and homogenization accounted for this improvement with a more uniform distribution of corrosion products and possible reduction of galvanic corrosion between ferrite and cementite.

The best combination of parameters for corrosion resistance was obtained at microstructures with acicular ferrite, as TMAZ and stir zone, that presented high corrosion potentials, polarization resistances and Tafel slopes. Although fine bainitic structure of hard zone developed the smallest corrosion current densities, its lower corrosion potential and high sensitivity to potential variation (small Tafel slopes) eventually led to pitting corrosion at grain boundaries, the most active sites due to lattice defects.

5. ACKNOWLEDGEMENTS

Authors thank Dr. Getúlio de Vasconcelos and MSc. Renê Volu, from Dedalo Laboratory at the Institute for Advanced Studies (IEAv), for their support with laser processing, CAPES, for graduation scholarship, and FAPESP, for research funding (Proc. 2016/10637-4).

6. REREFENCES

Mishra, R.S., and Z.Y. Ma. 2005. “Friction Stir Welding and Processing.” *Materials Science and Engineering: R: Reports*, Vol. 50, No. 1–2, pp. 1–78.

Padhy, G.K., C.S. Wu, and S. Gao. 2018. “Friction Stir Based Welding and Processing Technologies - Processes, Parameters, Microstructures and Applications: A Review.” *Journal of Materials Science & Technology*, Vol. 34, No. 1 1–38.

Defalco, B.Y.J., Steel, R. 2009. “Friction stir process now welds steel pipe”, *Welding Journal*, Vol. 5, pp. 44–48.

Santos, T.F.A., T.F.C. Hermenegildo, C.R.M. Afonso, R.R. Marinho, M.T.P. Paes, and A.J. Ramirez. 2010. “Fracture Toughness of ISO 3183 X80M (API 5L X80) Steel Friction Stir Welds.” *Engineering Fracture Mechanics*, Vol. 77, No. 15, pp. 2937–45.

Aydin, Hakan, and Tracy W. Nelson. 2013. “Microstructure and Mechanical Properties of Hard Zone in Friction Stir Welded X80 Pipeline Steel Relative to Different Heat Input.” *Materials Science and Engineering: A*, Vol. 586, pp. 313–22.

Sowards, Jeffrey W., Thomas Gnäupel-Herold, J. David McColskey, Victor F. Pereira, and Antonio J. Ramirez. 2015. “Characterization of Mechanical Properties, Fatigue-Crack Propagation, and Residual Stresses in a Microalloyed Pipeline-Steel Friction-Stir Weld.” *Materials & Design*, Vol. 88 pp. 632–42.

Avila, Julian A., Johnnatan Rodriguez, Paulo Roberto Mei, and Antonio J. Ramirez. 2016. “Microstructure and Fracture Toughness of Multipass Friction Stir Welded Joints of API-5L-X80 Steel Plates.” *Materials Science and Engineering: A*, Vol. 673, pp. 257–65.

Pao, P.S. Pao, Fonda, R.W., Jones, H.N., Feng, C.R., and Moon, D.W. 2007. *Friction Stir Welding of HSLA-65 Steel, Friction Stir Welding and Processing IV*, R.S. Mishra, M.W. Mahoney, T.J. Lienert, K.V. Jata, Eds., The Minerals Metals, and Materials Society, pp. 243-251.

Ralston, K.D., N. Birbilis, and C.H.J. Davies. 2010. “Revealing the Relationship between Grain Size and Corrosion Rate of Metals.” *Scripta Materialia*, Vol. 63 No 12, pp. 1201–4.

Jangir, Dinesh Kumar. 2018. “Influence of Grain Size on Corrosion Resistance and Electrochemical Behaviour of Mild Steel.” *International Journal for Research in Applied Science and Engineering Technology*, Vol. 6, No. 4, pp. 2875–81.

Mishra, Rajiv Sharan, Partha Sarathi De, and Nilesh Kumar. 2014. *Friction Stir Welding and Processing*. Springer International Publishing.

Böhni, H., T. Suter, and A. Schreyer. 1995. “Micro- and Nanotechniques to Study Localized Corrosion.” *Electrochimica Acta*, Vol. 40, No. 10, pp. 1361–68.

Suter, T., and H. Böhni. 1997. “A New Microelectrochemical Method to Study Pit Initiation on Stainless Steels.” *Electrochimica Acta*, Vol.42, No. 20-22, pp. 3275–80.

Andreatta, F., and L. Fedrizzi. 2016. “The Use of the Electrochemical Micro-Cell for the Investigation of Corrosion Phenomena.” *Electrochimica Acta*, Vol. 203, pp. 337–49.

Jariyaboon, M., A. J. Davenport, R. Ambat, B. J. Connolly, S. W. Williams, and D. A. Price. 2006. “Corrosion of a Dissimilar Friction Stir Weld Joining Aluminium Alloys AA2024 and AA7010.” *Corrosion Engineering, Science and Technology*, Vol. 41, No. 2, pp. 135–42.

Jariyaboon, M., A.J. Davenport, R. Ambat, B.J. Connolly, S.W. Williams, and D.A. Price. 2007. “The Effect of Welding Parameters on the Corrosion Behaviour of Friction Stir Welded AA2024–T351.” *Corrosion Science*, Vol. 49, No. 2, pp. 877–909.

Jariyaboon, M., A. J. Davenport, R. Ambat, B. J. Connolly, S. W. Williams, and D. A. Price. 2009. “The Effect of Cryogenic CO2cooling on Corrosion Behaviour of Friction Stir Welded AA2024-T351.” *Corrosion Engineering*, Science and Technology, Vol. 44, No. 6, pp. 425–32.

Jariyaboon, M., A.J. Davenport, R. Ambat, B.J. Connolly, S.W. Williams, and D.A. Price. 2010. “Effect of Cryogenic Cooling on Corrosion of Friction Stir Welded AA7010-T7651.” *Anti-Corrosion Methods and Materials*, Vol. 57, No. 2, pp. 83–89.

Pašti, Igor A., Tamara Lazarević-Pašti, and Slavko V. Mentus. 2012. “Switching between Voltammetry and Potentiometry in Order to Determine H+ or OH− Ion Concentration over the Entire pH Scale by Means of Tungsten Disk Electrode.” *Journal of Electroanalytical Chemistry*, Vol. 665, pp. 83–89.

Ferhat, M., Benchettara , A., Amara, S.E., Najjar, D. 2014. “Corrosion behaviour of Fe-C alloys in a sulfuric medium.” *Journal of Materials and Environmental Science*, Vol. 5, No. 4, pp. 1059–1068

Ochoa, Nathalie, Carlos Vega, Nadine Pébère, Jacques Lacaze, and Joaquín L. Brito. 2015. “CO2 Corrosion Resistance of Carbon Steel in Relation with Microstructure Changes.” *Materials Chemistry and Physics*, Vol. 156, pp. 198–205.

Alizadeh, Mostafa, and Sajjad Bordbar. 2013. “The Influence of Microstructure on the Protective Properties of the Corrosion Product Layer Generated on the Welded API X70 Steel in Chloride Solution.” *Corrosion Science*, Vol. 70, pp. 170–79.

Gollapudi, Srikant. 2012. “Grain Size Distribution Effects on the Corrosion Behaviour of Materials.” *Corrosion Science*, Vol. 62 (September): 90–94.

Hao, Xuehui, Junhua Dong, Ini-Ibehe Nabuk Etim, Jie Wei, and Wei Ke. 2016. “Sustained Effect of Remaining Cementite on the Corrosion Behavior of Ferrite-Pearlite Steel under the Simulated Bottom Plate Environment of Cargo Oil Tank.” *Corrosion Science*, Vol. 110, pp. 296–304.

Du, C.W., X.G. Li, P. Liang, Z.Y. Liu, G.F. Jia, and Y.F. Cheng. 2008. “Effects of Microstructure on Corrosion of X70 Pipe Steel in an Alkaline Soil.” *Journal of Materials Engineering and Performance*, Vol. 18, No. 2, pp. 216–20.

7. RESPONSIBILITY NOTICE

The authors are the only responsible for the printed material included in this paper.